Journal of Nuclear Materials 377 (2008) 65–71

Contents lists available at ScienceDirect

Journal of Nuclear Materials

journal homepage: www.elsevier.com/locate/jnucmat

The small ball punch test at FZJ

D. Finarelli [a], F. Carsughi [a,b,*], P. Jung [b]

[a] Università Politecnica della Marche, Dipartimento di Scienze Applicate ai Sistemi Complessi and INFM, Unit of Ancona, Italy
[b] Institut für Festkörperforschung, Forschungszentrum Jülich, Jülich, Germany

A B S T R A C T

The next generation of nuclear power reactors and neutron sources, together with the test devices for the fusion program, will pose an unprecedented severity of the environment for structural components near the irradiation sources. Therefore there is a need for material development and testing in the anticipated conditions and a number of institutions are involved in the process. A strong constraint in the volume of material available for testing, due to the high irradiation dose needed to meet proper conditions and the number of necessary samples, has driven the development of a number of tests to extract engineering properties from miniaturised specimens [G.E. Lucas, Metall. Trans. A 21 (1990) 1105, P. Jung, A. Hishinuma, G.E. Lucas, H. Ullmaier, J. Nucl. Mater. 232 (1996) 186]. The small ball punch (BP) test is a mechanical test for miniaturised samples. Although it is not yet a standard test, specimens discs dimensions of 3 mm diameter and 250 μm thickness are routinely used. The BP test finds application in the determination of elastoplastic and fracture properties of materials, such as the tensile strength, yield strength, fracture energy and ductile to brittle transition temperature (DBTT). Here a BP test apparatus developed at the Forschungszentrum Jülich with the contribution of the INFM is presented and its performance discussed.

1. Introduction

The small ball punch test (BP) is a well established experimental technique to determine the mechanical properties, ranging from elastic to fracture behaviour [1–4]. During the test a hard hemispherical head is pressed against a strongly constrained thin sheet until it is torn. A schematic view of BP operation is shown in Fig. 1. The typical experimental information is the load–displacement curve (L–d curve) of the head.

The BP test has found application, especially in the field of nuclear engineering and research, due to the very small sample required: typically a disc of 3 mm diameter and 250 μm thickness [5,6]. These dimensions help managing the volume constraints imposed on the material available for testing. These are related to the small irradiation volumes in the existing facilities, the large irradiation costs, beam gradient and the need to investigate the testing temperature and irradiated dose domain in order to have a full picture of the mechanical properties of the materials under irradiation.

The relationship between the L–d curve and the mechanical properties of material under investigation is not straightforward due to the complexity of the deformation process. Many semi-empirical relations have been proposed to quantify yield point, fracture strain and other engineering properties [5,7] and there have been a number of attempts to extract material's constitutive relations using a numerical simulation of the BP test with finite element methods together with an optimization process to solve the inverse problem [3,8].

Since the mechanical information available from the BP test is mainly associated with the plastic and fracture behaviour of the material, the identification of the crack opening and the observation of the fracture opening development during application of the load should afford a direct correlation with the L–d curve, and it opens the possibility for a unique and solid mechanical analysis of the fracture properties using FEM models which include also the fracture behaviour.

These features have been considered within the framework of the materials research for the European spallation source (ESS) program. Thus it was decided to improve the capabilities of the BP test available at the FZJ hot cells with a new device equipped to provide direct observation of crack development, a new capability in BP testing.

2. BP test at FZJ

The BP test apparatus at FZJ was designed with special attention to the following requirements:

(1) Observation of crack initiation and development.
(2) Applicability in hot cell environment.

* Corresponding author. Address: Institut für Festkörperforschung, Forschungszentrum Jülich, Jülich, Germany.
E-mail address: F.Carsughi@univpm.it (F. Carsughi).

0022-3115/$ - see front matter © 2008 Elsevier B.V. All rights reserved.
doi:10.1016/j.jnucmat.2008.02.053

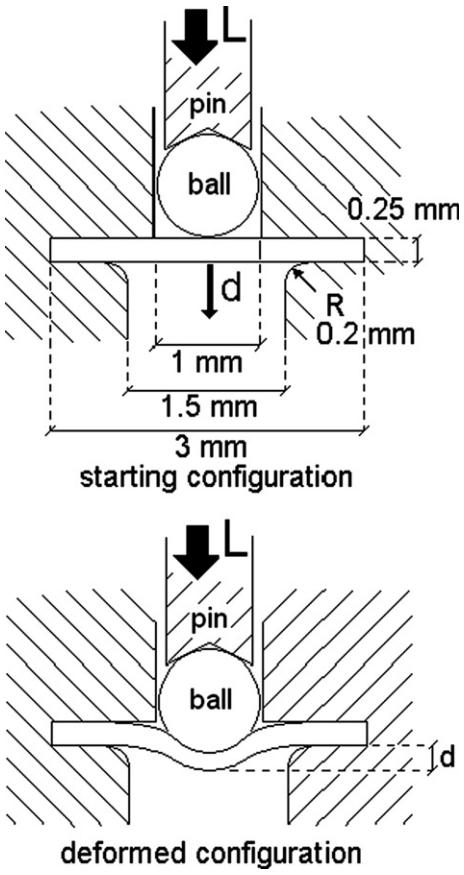

Fig. 1. BP operation principles.

(3) Displacement measurement resolution 1 μm.
(4) Load measurement error < 1%.
(5) Temperature range from −150 °C to 400 °C.
(6) Cost control.

The most important requirement is the observation of the lower face of the sample to follow crack evolution during the test operation. No electromechanical extensometer can be placed on this face and an optical system has been placed here to observe the sample surface. The surface to be observed is round, 1.5 mm of diameter, and the deformation connected to the pin tip penetration can reach almost 1 mm.

A camera has been employed to remotely observe the surface and a telescope is used for proper magnification of the small area under observation. To avoid direct view of the highly active specimen from the radiation sensitive digital camera, a mirror is used and the camera is placed to one side.

The temperature range, from −150 up to 400 °C requires a proper cooling and heating system. The system operates in a vacuum chamber, with the possible controlled gas atmosphere, to avoid icing on cold surfaces or contamination. The specimen anvil is equipped with an embedded pipe for nitrogen cooling and an electric heater. A thermocouple forms a ring around the specimen contact area and the temperature is controlled by an independent PID controller. The thermocouple is 3 mm from the sample and forms a full ring around it, the temperature is controlled within 2°. The vacuum system maintains a pressure of 10^{-6} mbar to minimize thermal dissipation from the sample.

The test load is applied to the sample from the punch head through a tungsten pin and a ball as shown in Fig. 1. The punch head moves to contact the pin that is centred by a conic hole. This

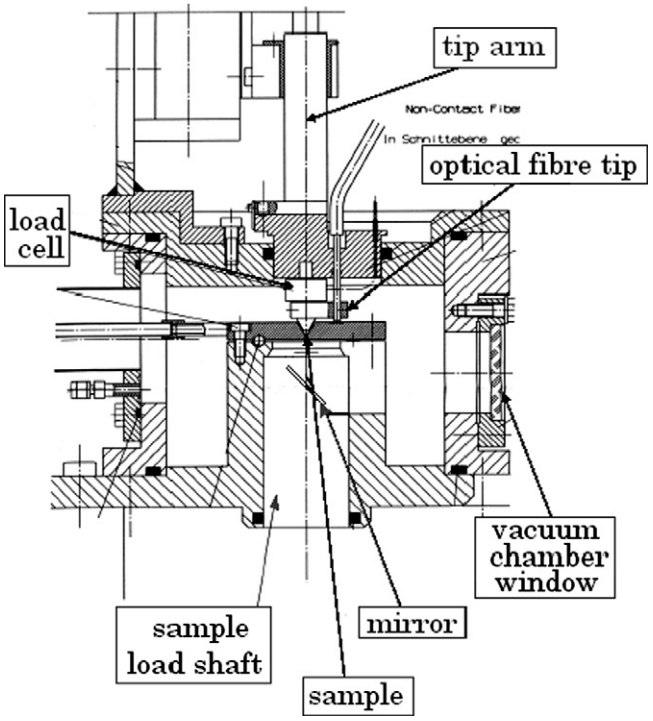

Fig. 2. Measurement chamber technical drawing, principal components are shown.

floating pin geometry minimizes the small off-center effects present in this technique and increases the precision of the load reading.

The displacement of the ball is detected with a fiber optic system from a Scantron model DMS D sensor: a mirror is located at the anvil surface and the optic fibre tip is tightly connected with the punch head just at the pin contact. This limits the uncertainty of the distance measurement to the elastic reaction of the tungsten pin. This optical sensor is designed for distances of several millimetres with a resolution of the order of 1 μm.

The load is acquired with a load cell positioned between the punch head and the punch arm.

The punch head is moved by a motorized linear table remotely controlled by a computer. The complete system is shown in Fig. 2.

The BP test device has been designed to work with highly radioactive specimens coming from irradiation programs, spent spallation targets or components discharged from nuclear reactors. Safe operation requires the manipulation of specimens to be executed in hot cells. To minimise and simplify operator movements, the specimen has to be inserted into a sample holder and the motorised lower arm loads the sample holder into the test area where the specimen is ready for testing.

The full experimental curve consists of several data points and the acquisition of each of them is found to be about 500 ms; this is due to the communication time between the computer and the DMS control via an rs232 port. Around 300 ms are necessary for consistent data acquisition. The distance measurement averages over 1024 acquisitions at a rate of 20 k sample/s; while the load measurement averages over 128 reading acquisitions at 1 k sample/s.

A schematic view of the electronic equipment and the computer control is shown in Fig. 3.

3. Operation

Each measurement is performed with the following steps:

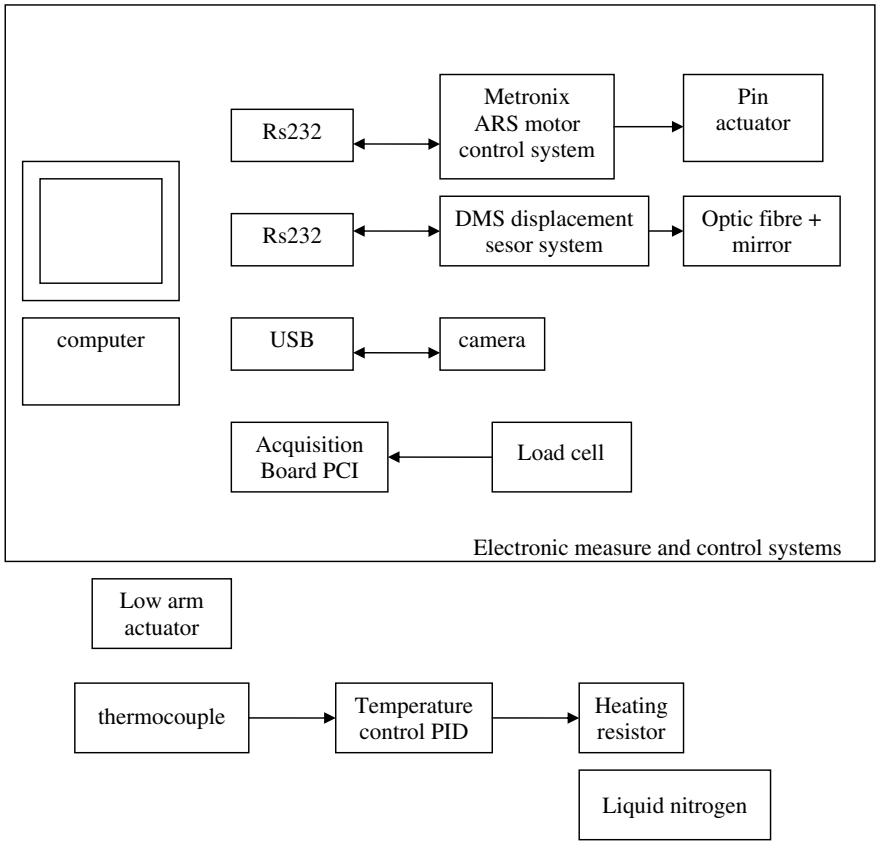

Fig. 3. Electronic acquisition and control systems scheme.

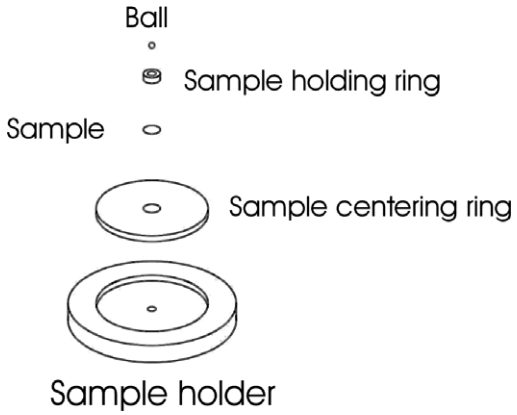

Fig. 4. Sample holder assembly.

(1) The operator prepares the sample, loads it in a sample holder together with the retention ring, the ball and the load pin. Fig. 4 shows the assembly. The sample holder is positioned on the lower arm and loaded against the bottom of the anvil.
(2) The punch head is lowered to hermetically close the vacuum chamber, it is positioned a millimeter from the load pin to avoid contact. The vacuum system is operated and proper pressure reached. The cooling/heating system is started and proper temperature reached.
(3) The automatic measurement is started, punch speed and travel is settled and the load–displacement curve is acquired. Optical observation from the camera is available and photos/videos can be acquired.
(4) The measurement stops, ambient temperature is re-established, ambient pressure is re-established, load arm raised, sample arm lowered, sample holder removed and disassembled, the broken sample is stored. The machine is ready for a new measurement.

4. BP apparatus commissioning

The BP apparatus has been operated on Optifer and Eurofer unirradiated specimens. The influence of vacuum, mechanical load and temperature on the load–displacement curves and the detector system has been evaluated: the machine stiffness is found to be 4–20 μm/100 kg.

Repeatability of the measurement, the influence of punch speed, sample thickness and ball material on the load–displacement curve have been evaluated.

Most of the tests have been performed using steel balls. Ball material influence has been evaluated on Eurofer samples. Three have been performed using Al_2O_3 ceramic balls and one using a transparent sapphire ball.

5. Sensor conditions

The effect of vacuum on the load cell reading has been evaluated using two Optifer samples with thickness of 250 ± 5 μm at ambient temperature. One measurement has been performed at ambient pressure, while the other at a pressure 10^{-6} mbar. The experimental curves are shown in Fig. 5, where no apparent influence can be observed.

The effect of temperature on the load cell reading has not been directly evaluated. Yet, for sample temperature −150 °C, load cell

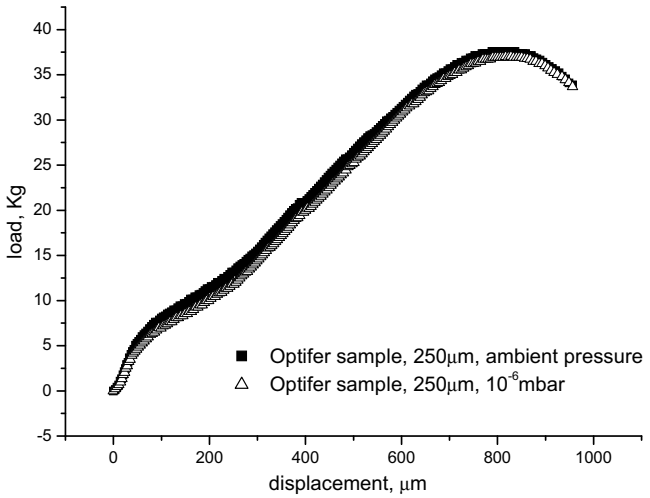

Fig. 5. Optifer specimens tested at different chamber pressure.

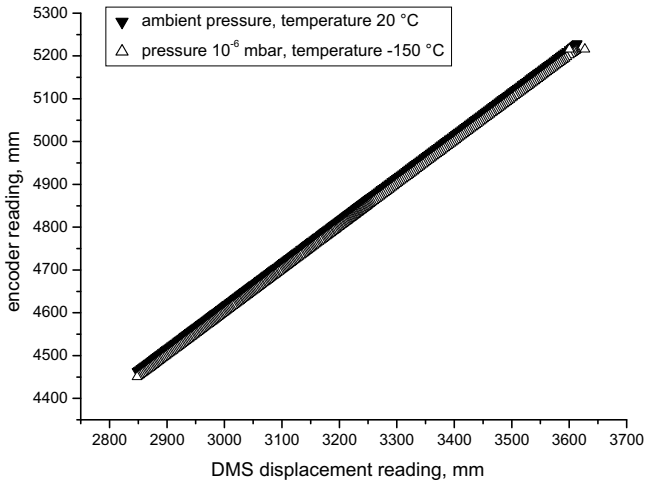

Fig. 6. DMS reading compared with encoder reading show direct proportionality between the distance evaluation and independence from pressure and temperature.

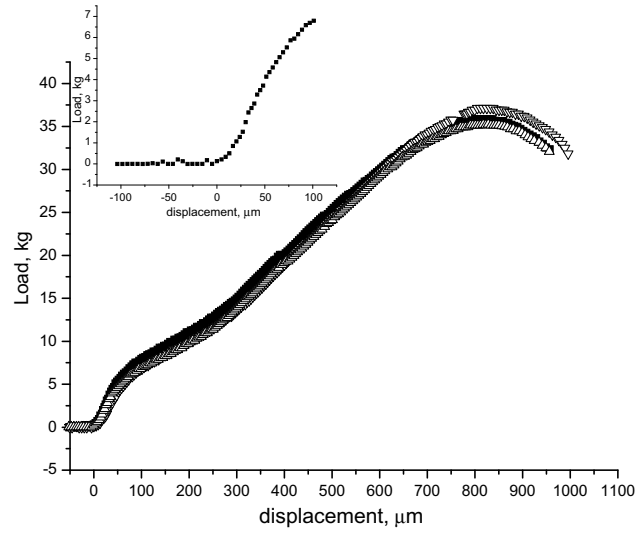

Fig. 7. Repeatability test on Optifer samples 250 ± 5 μm thickness, in the small box the detail of the contact definition of one of the test.

temperature is only 15 °C compared to 20 °C for ambient temperature. The effect of vacuum and temperature on the optical displacement reading has been evaluated by comparing the sensor reading with the encoder reading from the actuator. The data are shown in Fig. 6. No apparent influence can be observed.

6. Repeatability

A set of Optifer samples with thickness of 250 ± 5 μm has been employed to test the measurement repeatability. Four measurements have been performed occasionally during the month of operation time, at room temperature, using steel balls and 2 μm/s punch velocity. The repeatability results are excellent as shown in Fig. 7, where the small box details the contact region of one of the test.

7. Punch velocity

The effect of the punch velocity has been evaluated between 0.16 μm/s and 10 μm/s. The lower limit is fixed by the control system of the motorised linear table. The upper limit was arbitrarily defined allowing the operator to follow the sample surface changes under load. It can be observed in Fig. 8.

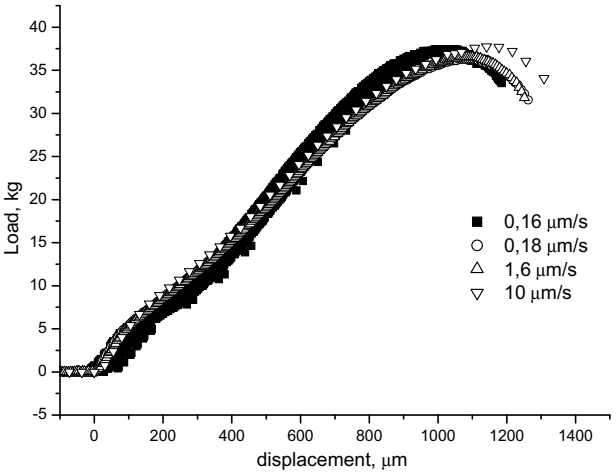

Fig. 8. Punch velocity effect on Optifer samples 250 ± 5 μm thickness.

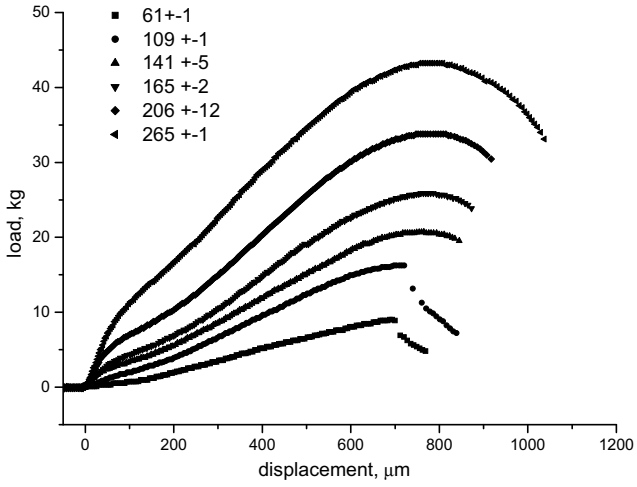

Fig. 9. Eurofer97 *P–d* curve for sample thickness ranging from 61 μm to 265 μm.

For the slowest velocity the acquisition of the load–displacement curve takes about 200 min, which limits the number of measurement to 2 samples per day. Moreover, since the picture acquisition is controlled by the operator, it is difficult to immediately perceive significant changes in the surface development.

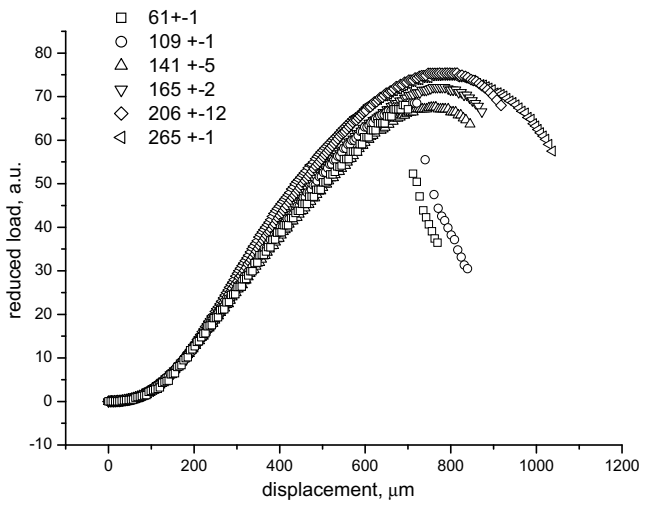

Fig. 10. Eurofer97 *P–d* curve for sample with thickness ranging from 61 μm to 265 μm reduced with function 1.

For the punch speed of 10 μm/s the acquisition of the experimental curve takes about 5 min and the full experimental time is dominated by the vacuum and thermal conditioning processes (about 30 min). The operator has no time to select interesting pictures especially near the crack, due to the very fast development of the surface.

It was found that the punch velocity of 1 μm/s is a good compromise, since the measurement takes about 30 min, which allows for picture acquisition and increases the possible number of experiments per day. Therefore, 1 μm/s was the punch velocity defined as standard. Naturally it is possible that other materials express a more pronounced velocity dependence that can need to be investigated.

8. Thickness dependence

Eurofer specimens have been used to investigate the thickness dependence of the load–displacement curve and the crack development during the application of the load.

A set of Eurofer specimens with thickness ranging from 61 μm up to 266 μm underwent the BP test. The results are shown in Fig. 9. The evolution of the *L–d* curve with the sample thickness is evident. Before the failure, a maximum in the *L–d* curve is visible only for sample thickness larger than 141 μm. The behaviour for small displacement depend on the, characteristic of the bending process, while for large displacement it is possible to scale the data with *d*, characteristic of the membrane stretching process. Therefore, an attempt to scale the *L–d* curves with different thicknesses has been performed by using the following normalization function:

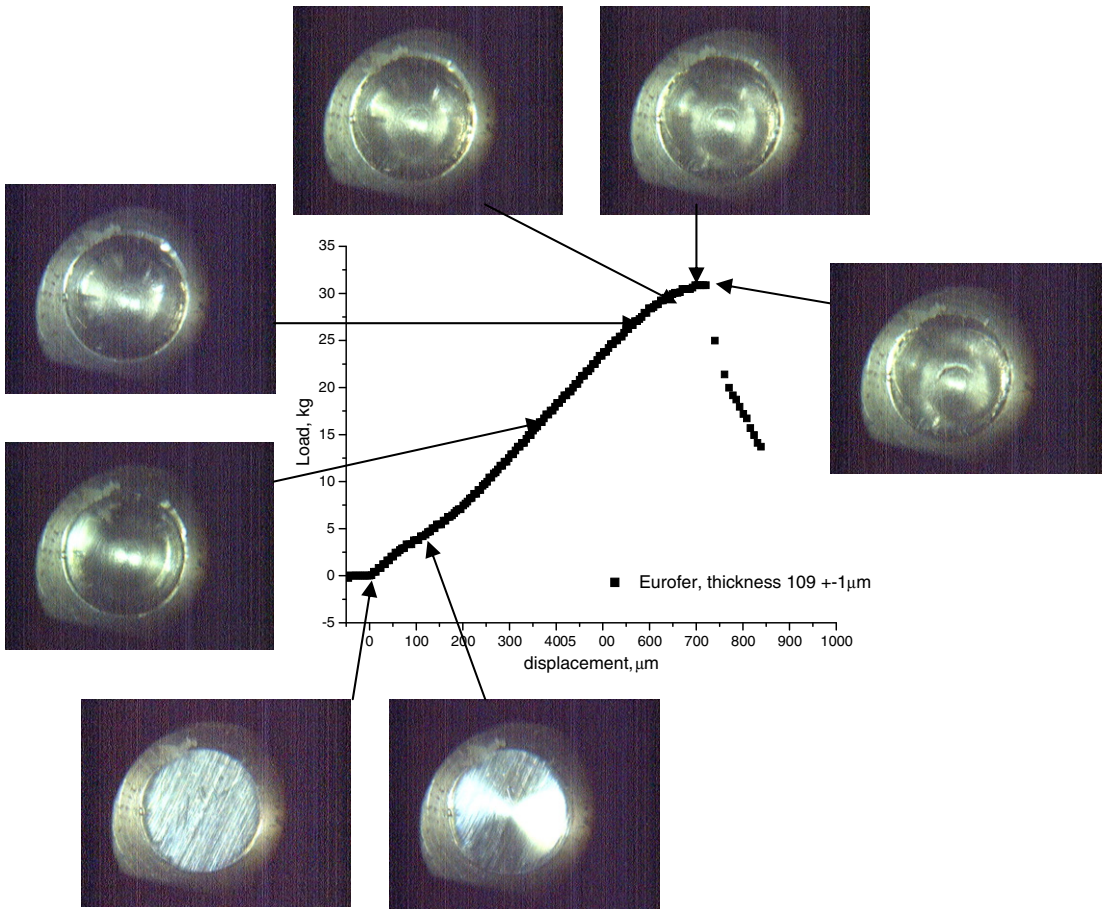

Fig. 11. Optical observation of specimen surface during the deformation process up to failure, pictures are acquired during the BP measurement, named after punch displacement and here arrow-linked to their proper position in the *L–d* curve.

$$L'(d) = \frac{L(d)}{d^{1+e^{-d/\delta_0}}}, \quad (1)$$

where δ_0 has a length dimension and represents the only fitting parameter. The best fit was found with $\delta_0 = 50 + th_0/5$, where th_0 is the nominal thickness.

The normalized data treated with function 1 are shown in Fig. 10.

The observation of the crack development is particularly visible for specimens of small thickness. Fig. 11 shows the load–displacement curve with the sample surface picture obtained at different displacements.

9. Ball material

Ball material introduces no visible change in the load–displacement curve for the present experimental configuration. The only difference we can report is a 'noisy' failure when using the ceramic and the sapphire balls, and a silent one with the steel ball. This is probably connected with the friction of the deformed surface on the punch ball; we do not have enough information at this time for more correlation of the ball material and effects.

10. Eurofer yield strength, fracture energy and DBTT

Eurofer samples have been investigated at different conditions: ambient temperature thickness effect on yield strength, using samples of thickness ranging from 61 to 266 μm, temperature effect on yield strength and fracture energy for sample thickness of 250 μm.

Eurofer yield strength σ_y is available from standard tensile test measurement at different temperature and these data are shown in Fig. 12 [9,10]. At 20 °C, yield strength of 550 MPa was found. Yield strength can be estimated from the load– displacement curves using semi-empirical relations as described in [4,5,7,11]

$$\sigma_y = \alpha \frac{P_A}{th_0^2}, \quad (2)$$

where α is fitting parameter and P_A the yield load. The parameter α was estimated by matching the tensile test data at ambient temperature [9,10] with the BP data at ambient temperature and different thickness; it was found to be 0.45, in good agreement with results from [4,7]. Yield strength for different temperatures were then evaluated using $\alpha = 0.45$ and are shown in Fig. 12, with a comparison with results from [9,10].

Fracture properties can include fracture energy, fracture length, thickness at fracture. Fracture energy has been calculated from load–displacement curves up to displacement at failure, neglecting the elastic recovery energy. During solicitation, fracture propagates along an arc until failure occurs, fracture length is the observable fracture arc length measured from pictures realized with the camera system during the punch displacement application.

The thickness at fracture edge is evaluated considering the equivalent fracture strain 1.5 [4,12], compatible with fracture ductile behaviour.

Table 2 compiles fracture properties for ambient temperature measurements on specimens thickness from 61 to 165 μm; fracture area is derived from fracture length and thickness at fracture. Fracture energy density behaviour for different thickness highlights the 'thin plate' geometry condition.

Ductile to brittle transition temperature (DBTT) for Eurofer is expected around −57 °C, [9] from Charpy test, and is connected to the collapse of fracture energy. Measurement performed on

Table 1
Yield strength evaluation for Eurofer97 SP test

Thickness, μm	266	206	165	141
P_A, kg	9	5	3.2	2.5
σ_y, MPa $\alpha = 0.45$	576	530	529	565

Table 2
Fracture length, thickness at fracture, energy at fracture, energy density

Sample thickness, μm	61	109	141	165
Fracture length, mm	0.55	0.6	0.7	0.75
Fracture thickness, μm	13.6	24.33	31.47	36.83
Energy at fracture, J	0.02952	0.05905	0.09967	0.1305
Energy density, J/mm^2	3.942	4.045	4.524	4.724

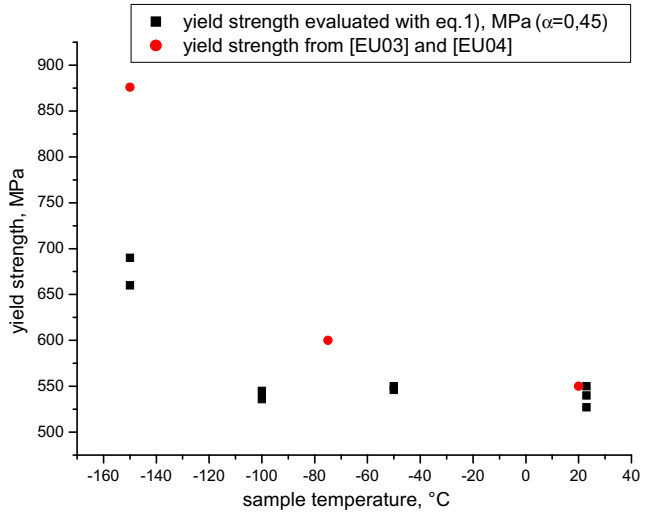

Fig. 12. Yield strength at different temperature for Eurofer97, as evaluated with BP test and Eq. (2) with $\alpha = 0.45$ (black square) compared with results from [9,10] (red prism). (For interpretation of the references to colour in this figure legend, the reader is referred to the web version of this article.)

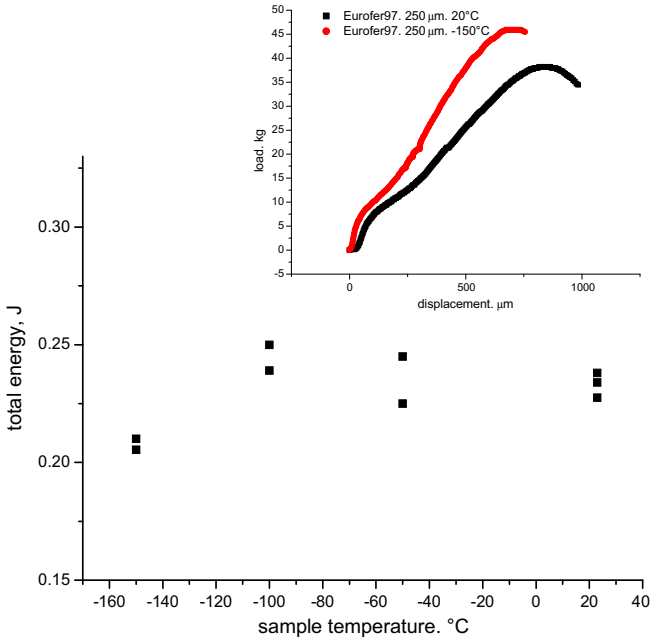

Fig. 13. Failure energy, integral under L–d curve up to failure, for 250 μm thickness Eurofer specimens BP tested at different temperatures. Two L–d curves for measurements at 20 °C and −150 °C are shown in the inset.

250 μm thickness specimens at various temperature as low as −150 °C have been performed. Fig. 13 shows fracture energy calculated from load–displacement curves together with 2 load–displacement curves, a 20 °C and a −150 °C test temperature. Low temperature curve shape is still connected to ductile failure (i.e. flat behaviour is still present on the top of the curve) and fracture energy is reduced but not collapsed (see Table 1).

11. Conclusions

The BP test machine at FZJ allows to perform consistent measurement with the required resolution and detail quality. The possibility of direct observation of the surface and crack development has been demonstrated with the possibility to correlate fracture propagation with punch displacement and the load–displacement curve.

Yield strength evaluation at ambient temperature using relation from [4,5,7,11] is consistent in a large thickness range, and the fitting parameter α is found 0.45; however this value was found to be less efficient for lower temperature.

A significant reduction of the fracture energy was observed for measurements at −150 °C.

References

[1] G.E. Lucas, Metall. Trans. A 21 (1990) 1105.
[2] P. Jung, A. Hishinuma, G.E. Lucas, H. Ullmaier, J. Nucl. Mater. 232 (1996) 186.
[3] M.P. Manahan, PhD dissertation MIT, Boston, 1982.
[4] D. Finarelli, M. Roedig, F. Carsughi, J. Nucl. Mater. 328 (2004) 146.
[5] X. Mao, H. Takahashi, J. Nucl. Mater. 150 (1987) 42.
[6] Y. Dai, X.J. Jia, K. Farrell, J. Nucl. Mater. 318 (2003) 192.
[7] Y. Ruan, P. Spatig, M. Victoria, J. Nucl. Mater. 307–311 (2002) 236.
[8] J. Foulds, C. Sainte Catherine et al., in: M.K. Sokolov, J.D. Landes, G.E. Lucas (Eds.), ASTM STP 1418, p. 350.
[9] E. Lucon, R. Chaouadi, SCK-CEN-BLG-945, 2003.
[10] A.-A.F. Tavassoli, A. Alamo, L. Bedel, et al., J. Nucl. Mater. 329–333 (2004) 257.
[11] V. Vorlivek, L.F. Exworthy, P.E. Flewitt, J. Mater. Sci. 30 (1995) 2936.
[12] J. Chakrabarty, Int. J. Mech. Sci. 12 (1970) 315.